INTERNATIONAL JOURNAL FOR NUMERICAL METHODS IN FLUIDS
*Int. J. Numer. Meth. Fluids* 2004; **44**:197–208 (DOI: 10.1002/fld.635)

# Euler solutions for aerodynamic inverse shape design

A. L. de Bortoli*,† and R. de Quadros

*Federal University of Rio Grande do Sul-UFRGS/PPGMAp, Bento Gonçalves 9500, 91509-900, Porto Alegre-RS, Brazil*

SUMMARY

Contributions to the aerodynamics development have to be involved to achieve an increase in quality, reducing time and computer costs. Therefore, this work develops an optimization method based on the finite volume explicit Runge–Kutta multi-stage scheme with central spatial discretization in combination with multigrid and preconditioning. The multigrid approach includes local time-stepping and residual smoothing. Such a method allows getting the goal of compressible and almost incompressible solution of fluid flows, having a rate of convergence almost independent from the Mach number. Numerical tests are carried out for the NACA 0012 and 0009 airfoils and three-dimensional wings based on NACA profiles for Mach-numbers ranging from 0.8 to 0.002 using the Euler equations. These calculations are found to compare favorably with experimental and numerical data available in the literature. Besides, it is worth pointing out that these results build on earlier ones when finding appropriate new three-dimensional aerodynamical geometries. Copyright © 2004 John Wiley & Sons, Ltd.

KEY WORDS: aerodynamics; optimization; (in)compressible flows; finite volumes; Runge–Kutta

## 1. INTRODUCTION

The major considerations in the design of effective methods for the computation of aerodynamics are the capability to treat flows over complex geometrical shapes with proper representation of shock waves or discontinuities. The design of aerodynamic bodies involves the calculation of the flow passing through various regimes, what is being possible due to powerful computers and user facilities.

There has been a considerable development of modern computational methods, but much work still remains to obtain fast, accurate and stable convergence techniques for all flow regimes. Besides, to efficiently solve problems which require fine grids, techniques to accelerate the convergence are required [1]. Approaches like local time-stepping, residual averaging and multigrid are widely applied.

Common numerical methods employed to solve fluid flows are the finite differences, finite volume, finite elements, boundary elements and spectral techniques. Each of these methods

* Correspondence to: A. L. de Bortoli, Department of Pure and Applied Mathematics, Federal University of Rio Grande do Sul, Av. Bento Gonçalves 9500, 90509-900, Porto Alegre-RS, Brazil.
† E-mail: dbortoli@mat.ufrgs.br

*Received December 1998*
*Revised 5 August 2003*

has its own advantages and disadvantages, which are not discussed in this work; they are being successfully used by known researches all over the world. Nevertheless, all methods employed to solve flows have the common feature that the domain has to be divided into a number of small cells of appropriate shape. The solution of the global system of equations delivers the variables at the mesh points (cells, elements).

This work presents an efficient method for the solution of (in)compressible flows based on the finite volume explicit Runge–Kutta [2] five-stages scheme. The severe time-step restriction of the explicit conventional methods is relaxed by the enlarged stability region of the Runge–Kutta scheme. Besides, to eliminate difficulties of the standard compressible method, when solving incompressible flows, preconditioning is employed [3, 4].

Aerodynamic optimization is also here considered. This can be done as a shape optimization or an inverse shape design. The first attempts to find the best aerodynamic property from the design. The inverse approach requires that a local property, of the final configuration, be specified as a goal of the design. Here, for a given surface pressure, the objective is to find the shape which will achieve such distribution. This is best done coupling the flow analysis and the shape modification.

Numerical tests are carried out for the NACA 0012 and 0009 airfoils and wing configurations based on NACA profiles for Mach numbers ranging from 0.8 to 0.002 using the Euler equations. The code is calibrated using potential/analytical equation solutions or experimental data found in the literature.

## 2. GOVERNING EQUATIONS

The adequate set of governing equations for non viscous flows are the Euler equations, in which mass, momentum and energy are conserved. They can be written for unsteady three-dimensional compressible flows in differential form as

$$\frac{\partial \mathbf{W}}{\partial t} + \frac{\partial \mathbf{F}_1}{\partial x} + \frac{\partial \mathbf{F}_2}{\partial y} + \frac{\partial \mathbf{F}_3}{\partial z} = 0 \tag{1}$$

where

$$\mathbf{W} = \begin{Bmatrix} \rho \\ \rho u \\ \rho v \\ \rho w \\ \rho E \end{Bmatrix}, \quad \bar{\bar{F}} = \begin{Bmatrix} \rho \mathbf{q} \\ \rho u \mathbf{q} + p.\mathbf{i} \\ \rho v \mathbf{q} + p.\mathbf{j} \\ \rho w \mathbf{q} + p.\mathbf{k} \\ \rho H \mathbf{q} \end{Bmatrix}, \quad \bar{\bar{F}} = \mathbf{F}_1\mathbf{i} + \mathbf{F}_2\mathbf{j} + \mathbf{F}_3\mathbf{k}$$

and $\rho$ is the fluid density, $\mathbf{q}$ the velocity vector ($\mathbf{q} = u\mathbf{i} + v\mathbf{j} + w\mathbf{k}$) and $p$ the pressure.

Since the integral form of conservation laws allow discontinuities, the approach is suitable for capturing shocks in the flow field. The total energy $E$ and enthalpy $H$ are given by

$$E = e + \frac{u^2 + v^2 + w^2}{2}, \quad H = E + \frac{p}{\rho} \tag{2}$$

 

where $e$ is the internal energy. To close this system of equations, the state relation for a perfect gas is employed

$$p = \rho RT = (\gamma - 1)\rho \left( E - \frac{u^2 + v^2 + w^2}{2} \right) \tag{3}$$

where $R$ is the gas constant and $\gamma$ the specific heat ratio. Equation (1) can be cast into the integral form

$$\int_V \frac{\partial \mathbf{W}}{\partial t} \, \mathrm{d}V + \int_S (\bar{\bar{F}}.\mathbf{n}) \, \mathrm{d}S = 0 \tag{4}$$

It is known that the time-marching schemes developed to compressible flows converge very slowly when the magnitude of velocity becomes small, in comparison with the acoustic speed [4]. Therefore, preconditioning is employed here and consist basically in multiplying the vector $\mathbf{W}$ from Equation (1) by a special matrix, which modifies the form of the governing equations. It has the advantage to ensure rapid convergence and allows solving for various flow regimes. Based on the conservation variables, the following matrix $\Gamma$ is adopted:

$$\Gamma \frac{\partial \mathbf{W}}{\partial t} + \frac{\partial \mathbf{F}_1}{\partial x} + \frac{\partial \mathbf{F}_2}{\partial y} + \frac{\partial \mathbf{F}_3}{\partial z} = 0 \tag{5}$$

where [2], for $q^2 = \mathbf{q}.\mathbf{q}$ and $C = 1 - M^{-2}$

$$\Gamma = \begin{bmatrix} 1 & 0 & 0 & 0 & 0 \\ 0 & 1 & 0 & 0 & 0 \\ 0 & 0 & 1 & 0 & 0 \\ 0 & 0 & 0 & 1 & 0 \\ \frac{-q^2 C}{2} & uC & vC & wC & M^{-2} \end{bmatrix}$$

This matrix indicates that the energy equation is transformed into a temperature equation for low Mach numbers. Thus, the eigenvalues of the resultant system of equations will be very similar when the Mach number goes to zero, laying the basis of construction of efficient solvers also to solve incompressible or mixed flows [3, 4].

## 3. DESCRIPTION OF THE NUMERICAL METHOD

One of the differences among the various finite volume formulations known in the literature is the arrangement of the control volume and update points for the flow variables [5]. The most frequently used schemes are the cell-centred, cell-vertex and node-centred approach; they are similar. Each of these schemes has its own advantages and disadvantages. The discretization preferred here is based on the node-centred arrangement [6], as shown in Figure 1.

 

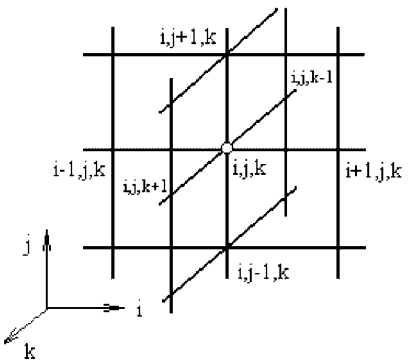


Figure 1. Node-centred arrangement.

In the computational domain the cell vertices are identified by their indices $(i, j, k)$. As Equation (1) is valid for arbitrary control volume, it is also valid for $V_{i,j,k}$, that means

$$\frac{\partial \mathbf{W}_{i,j,k}}{\partial t} = -\frac{1}{V_{i,j,k}} \int_S (\bar{\bar{F}}.\mathbf{n})\, \mathrm{d}S \tag{6}$$

The finite volume discretization based on the central averaging is not dissipative. Convergence to the steady state solution is difficult when the high frequency oscillations of error, in each step of the solution procedure, are not damped; to avoid these oscillations dissipative terms $\mathbf{D}_{i,j,k}$ are introduced. The optimum amount of artificial viscosity is mainly determined by the smoothing properties of relaxation and is written as follows [5]:

$$\frac{\partial \mathbf{W}_{i,j,k}}{\partial t} + \frac{1}{V_{i,j,k}}[\mathbf{Q}_{i,j,k} - \mathbf{D}_{i,j,k}] = 0 \tag{7}$$

This dissipation operator is a blend of second and fourth differences and is defined according to

$$\mathbf{D}_{i,j,k} = \mathbf{d}_{i,j+1/2,k} - \mathbf{d}_{i,j-1/2,k} + \mathbf{d}_{i+1/2,j,k} - \mathbf{d}_{i-1/2,j,k} + \mathbf{d}_{i,j,k+1/2} - \mathbf{d}_{i,j,k-1/2} \tag{8}$$

whose dissipation coefficient is given by

$$\mathbf{d}_{i+1/2,j,k} = \alpha_{i+1/2,j,k}[\varepsilon^2_{i+1/2,j,k}\delta_x \mathbf{W}_{i,j,k} - \varepsilon^4_{i+1/2,j,k}\delta_{xxx}\mathbf{W}_{i-1,j,k}] \tag{9}$$

The difference operators of first and third order are $\delta_x$ and $\delta_{xxx}$, respectively, and $\alpha$ is the scaling factor, which is written for **i** direction in the following way [6]

$$\alpha_{i+1/2,j,k} = \tfrac{1}{2}(\lambda^{i^+}_{i,j,k} + \lambda^{i^+}_{i+1,j,k}) \tag{10}$$

where

$$\lambda^{i^+}_{i,j,k} = \lambda^i_{i,j,k}\phi^i_{i,j,k}, \quad \phi^i_{i,j,k} = 1 + \max\left[\left(\frac{\lambda^j_{i,j,k}}{\lambda^i_{i,j,k}}\right)^\omega, \left(\frac{\lambda^k_{i,j,k}}{\lambda^i_{i,j,k}}\right)^\omega\right] \tag{11}$$

and $w$ is a parameter used to scale the spectral radii.

 

The coefficients, adapted to the local pressure gradients $\varepsilon^2$ and $\varepsilon^4$, needed to obtain the dissipation, are given by

$$\varepsilon^2_{i+1/2,j,k} = K^2 \max(v_{\max}) \tag{12}$$

$$\varepsilon^4_{i+1/2,j,k} = \max(0, K^4 - \varepsilon^2_{i+1/2,j,k}) \tag{13}$$

where

$$v_{\max} = (v_{i+2,j,k}, v_{i+1,j,k}, v_{i,j,k}, v_{i-1,j,k}), \quad v_{i,j,k} = \left| \frac{p_{i+1,j,k} - 2p_{i,j,k} + p_{i-1,j,k}}{p_{i+1,j,k} + 2p_{i,j,k} + p_{i-1,j,k}} \right| \tag{14}$$

and

$$0.5 \leqslant K^2 \leqslant 0.6, \quad \frac{1}{128} \leqslant K^4 \leqslant \frac{1}{48}$$

The coefficient $\varepsilon^4$ provides the background dissipation in smooth parts of the flow and can be used to improve the capability of the scheme to damp high frequency modes. The spectral radius $\lambda$, used to control the amount of artificial dissipation, is defined for the **i** direction according to [3]

$$\lambda^i = \frac{u(1+M^2) + \sqrt{u^2(1-M^2)^2 + \beta^2 c^2}}{2} \tag{15}$$

To avoid zero artificial dissipation viscosity $\beta^2$ is chosen as $\beta^2 = \max(4M^2, \phi)$, where $0.1 \leqslant \phi \leqslant 0.6$ [4].

### 3.1. Time-stepping and acceleration techniques

To obtain numerical solutions of high accuracy, the Runge–Kutta method is chosen [2, 5]. It is characterized by its low operation count; more than two stages are employed to extend the stability region [5]. The classical fourth order Runge–Kutta method requires the evaluation of many coefficients and dissipative terms, what leads to storage problems. Therefore, the following multistage scheme, which requires little computational storage, is employed [5]:

$$\begin{aligned} \mathbf{W}^{(0)}_{i,j,k} &= \mathbf{W}^{(n)}_{i,j,k} \\ \mathbf{W}^{(r)}_{i,j,k} &= \mathbf{W}^{(0)}_{i,j,k} - \frac{\alpha_r \Delta t}{V_{i,j,k}} R^{(r-1)}_{i,j,k} \\ \mathbf{W}^{(n+1)}_{i,j,k} &= \mathbf{W}^{(r)}_{i,j,k} \end{aligned} \tag{16}$$

where $\mathbf{R}^{(r)}_{i,j,k} = \mathbf{Q}^{(r)}_{i,j,k} - \mathbf{D}^{(r)}_{i,j,k}$, $r = 1, 2, \ldots, m = 5$.

The search for efficient methods to solve flows is obvious (justified). Among the approaches available to solve them, the local time-stepping, residual averaging and its combination with multigrid are here adopted. Local time-stepping is equivalent to preconditioning the residual by a scalar value in each cell; it can reduce the computational time needed to obtain steady state solutions by an order of magnitude. A weighted average of residuals is employed to increase the Courant–Friedrichs–Lewy number of an explicit multistage scheme. In this way, the residuals are replaced by an average of neighbouring residuals [5].

 

The slow asymptotic convergence of numerical methods is associated to the smooth error components. The good smoothing properties of the Runge–Kutta method, especially of the 5-stage scheme, are very important to be used in a multigrid solver. The success of the multigrid method depends on the use of a relaxation algorithm [1], which rapidly reduces the high frequency error components. The low error frequencies in fine meshes are transformed in high frequencies in coarse meshes, where they can be better smoothed.

The computational procedure to illustrate the FAS (full approximation storage) for two grids is written as follows [1, 4]:

(1) Improve the solution on the finest grid.
(2) Inject the variables from the fine to the coarse grid.
(3) Transfer the residuals from the fine to the coarse grid.
(4) Solve the problem on the coarse grid.
(5) Interpolate the solution correction from the coarse to the fine mesh.
(6) Update the solution on the finest grid.

The most important point of the coarse-to-fine correction interpolation and the residual transfer is their orders; thus, bilinear interpolation has order two and is used. Besides, high frequency errors are the most expensive to liquidate in the multigrid cycling, since they are processed on the finest grid.

In practice, if $W$-cycles have good convergence properties, usually $V$-cycles may also be used. Often, the convergence properties of $V$-cycles are worse than those from $W$-cycles. For low Mach numbers difficulties appear to smooth the low frequencies of error, slowing down the convergence. This occurs because the eigenvalues of the incompressible equations are similar when the Mach numbers goes to zero. To alleviate this problem more work is done on the coarse meshes, using a $W$-multigrid cycle [4].

### *3.2. Boundary conditions*

The numerical treatment of boundary conditions is one of the major problems when solving the Euler equations. Inappropriate conditions can substantially degrade the accuracy and convergence of the computed solution. Numerical conditions imposed on the outer boundary should assure that the outgoing waves are not reflected back into the flow field. To establish an efficient numerical implementation of the boundary conditions the computational domain is surrounded by dummy cells. Straight lines approximate the body coinciding with a coordinate system. On a solid body, the physical condition of no normal flow can be imposed. Since the numerical treatment of the flow exterior to a body such as an airfoil requires a bounded domain, an artificial far field is introduced.

The approach used at far field boundaries [7] is based on the characteristic form of the one dimensional Euler equations normal to the boundary. As the far field boundary condition assumes zero circulation, the boundary has to be placed sufficiently far away from the airfoil (20–30 chord lengths), so the flow field remains undisturbed.

### *3.3. Inverse shape design*

The optimization of aerodynamic geometries can be classified in two categories: the direct and the inverse. The first intents to find the best global aerodynamic property. The inverse

 

form requires a local property ($C_p$ for example) of the final configuration as the objective of development.

From a given airfoil such as the NACA 0012, whose pressure coefficient is well known for various flow regimes, it is desired to find a new shape that minimize shocks; the advantage of the finite volume implementation in this context is that the flux is locally verified, in agreement with the idea of the inverse design for the attainment of the body geometry.

To the shape evolution, using the elastic membrane technique [8, 9], one separates the upper and lower sides of the airfoil (wing cross-section). On the upper side the Fourier serie results

$$-\alpha_0 \Delta y + \alpha_1 \frac{\mathrm{d}\Delta y}{\mathrm{d}s} + \alpha_2 \frac{\mathrm{d}^2 \Delta y}{\mathrm{d}s^2} = \Delta C_p \tag{17}$$

and similarly on the lower airfoil contour (only changing the sign of $\alpha_0$), where $s$ is the airfoil contour coordinate, $\Delta C_p$ the pressure coefficient difference between the desired and that at actual iteration and the $\alpha_i$'s are user constants that control the rate of convergence of the shape evolution process.

These two ordinary differential equations, with constant coefficients, come from the well known forced mass-spring-damper system. The $\Delta C_p$ in Equations (17) can be represented using Fourier series expansion of the form

$$\Delta C_p = a_0 + \sum_{n=1}^{n_{\max}} [a_n \cos(N_n s) + b_n \sin(N_n s)] \tag{18}$$

where $N_n = 2\pi n/l$ and $l$ is the total length of the airfoil contour.

The particular solution of Equation (17) can be represented in the Fourier series form as

$$\Delta y_p = A_0 + \sum_{n=1}^{n_{\max}} [A_n \cos(N_n s) + B_n \sin(N_n s)] \tag{19}$$

Since the Fourier coefficients ($A_n$ and $B_n$) of the particular solutions on the upper and lower airfoil contours are different, it can be expected that gaps will form at the leading and trailing edges of the airfoil. These gaps can be closed with appropriate homogeneous solutions.

The upper contour homogeneous solution is

$$\Delta y_h^{\mathrm{top}} = F^{\mathrm{top}} \mathrm{e}^{\lambda_1 s} + G^{\mathrm{top}} \mathrm{e}^{\lambda_2 s} \tag{20}$$

where

$$\lambda_{1,2} = \frac{\alpha_1 \pm \sqrt{{\alpha_1}^2 + 4\alpha_0 \alpha_2}}{2\alpha_2} \tag{21}$$

and $F^{\mathrm{top}}$ and $G^{\mathrm{top}}$ are coefficients to be determined. Likewise, on the lower airfoil contour, the homogeneous solution is

$$\Delta y_h^{\mathrm{bot}} = F^{\mathrm{bot}} \mathrm{e}^{-\lambda_1 s} + G^{\mathrm{bot}} \mathrm{e}^{-\lambda_2 s} \tag{22}$$

 

Thus, the overall displacement of the airfoil contour is given by the following equations:

$$\Delta y^{\text{top}} = F^{\text{top}} e^{\lambda_1 s} + G^{\text{top}} e^{\lambda_2 s} + \sum_{n=1}^{n_{\max}} [A_n^{\text{top}} \cos(N_n s) + B_n^{\text{top}} \sin(N_n s)] \tag{23}$$

$$\Delta y^{\text{bot}} = F^{\text{bot}} e^{-\lambda_1 s} + G^{\text{bot}} e^{-\lambda_2 s} + \sum_{n=1}^{n_{\max}} [A_n^{\text{bot}} \cos(N_n s) + B_n^{\text{bot}} \sin(N_n s)] \tag{24}$$

The four unknown constants $F^{\text{top,bot}}$ and $G^{\text{top,bot}}$ can now be determined for the upper and lower airfoil contours. The convergence depends mainly on the leading and trailing edges of the airfoil convergence, where the following conditions are adopted for:

- trailing edge displacement: $\Delta y^{\text{bot}}(0) = 0$;
- trailing edge closure: $\Delta y^{\text{bot}}(0) = \Delta y^{\text{top}}(L)$,
- leading edge closure: $\Delta y^{\text{bot}}(S_{\text{le}}) = \Delta y^{\text{top}}(S_{\text{le}})$ and
- smooth leading edge deformation: $\mathrm{d}[\Delta y^{\text{bot}}(S_{\text{le}})]/\mathrm{d}s = \mathrm{d}[\Delta y^{\text{top}}(S_{\text{le}})]/\mathrm{d}s$.

where $\Delta y$ is the $y$-direction co-ordinate variation, $l$ the total length of the airfoil contour and $S_{\text{le}}$ the value of the contour at the leading edge.

Using the previous equations simultaneously, for the unknown coefficients $F$ and $G$, results in

$$\begin{Bmatrix} F^{\text{bot}} \\ G^{\text{bot}} \\ F^{\text{top}} \\ G^{\text{top}} \end{Bmatrix} \begin{bmatrix} 1 & 1 & 0 & 0 \\ 0 & 0 & e^{l\lambda_1} & e^{l\lambda_2} \\ e^{-S_{\text{le}}\lambda_1} & e^{-S_{\text{le}}\lambda_2} & -e^{S_{\text{le}}\lambda_1} & -e^{S_{\text{le}}\lambda_2} \\ -\lambda_1 e^{-S_{\text{le}}\lambda_1} & -\lambda_2 e^{-S_{\text{le}}\lambda_2} & -\lambda_1 e^{S_{\text{le}}\lambda_1} & -\lambda_2 e^{S_{\text{le}}\lambda_2} \end{bmatrix}$$

$$= \begin{Bmatrix} -\sum_{n=0}^{n_{\max}} A_n^{\text{bot}} \\ -\sum_{n=0}^{n_{\max}} A_n^{\text{top}} \\ \sum_{n=0}^{n_{\max}} [\Delta A_n \cos(N_n S_{\text{le}}) + \Delta B_n \sin(N_n S_{\text{le}})] \\ \sum_{n=0}^{n_{\max}} [-N_n \Delta A_n \sin(N_n S_{\text{le}}) + N_n \Delta B_n \cos(N_n S_{\text{le}})] \end{Bmatrix}$$

The two-dimensional Fourier series shape evolution equation can be expanded to three dimensions, expressing values to $k$-planes as in the bidimensional case. Such procedure reduces considerably the computational effort.

## 4. NUMERICAL RESULTS

In the following, numerical results for NACA 0012, 0009, a new airfoil and wings are presented. The first simulation is concerned to an airfoil submitted to incompressible flow. The

 

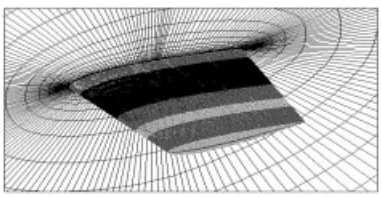

Figure 2. Mesh for wing, $160 \times 64 \times 20$.

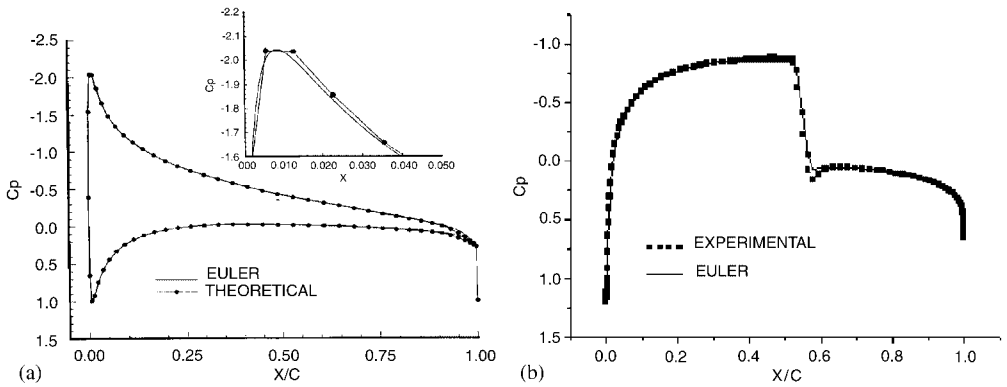


Figure 3. Pressure coefficient for NACA 0012; (a) Mach $= 0.002$, $\alpha = 5^\circ$ and (b) Mach $= 0.8$, $\alpha = 0^\circ$.

calculations have been carried out on a O-type grid which consists of $160 \times 64$ cells, as a section presented in Figure 2. The position of the outer boundary is around thirty chord lengths away from the airfoil. Five grids and a $W$-cycle are used in the multigrid process ($160 \times 64$—fine grid, $80 \times 32$—second grid, $40 \times 16$—third grid, $20 \times 8$—fourth grid, $10 \times 4$—fifth grid). The most important and frequently used choice of the coarse mesh is characterized by doubling the given mesh size ($H = 2h$), which is called standard coarsening. The value two is the smallest recursively convenient number and is big enough to make the coarse grid work small relative to the fine grid work.

In order to check the numerical code, results for the NACA 0012 airfoil are compared to a solution obtained by the conforming mapping technique [6] for incompressible flow (Mach 0.002) and with experiments for compressible flows (Mach=0.8) [4]. Figure 3(a) shows the pressure coefficient computed for Mach=0.002 and $\alpha = 5^\circ$ (incompressible flow). The overall accuracy is quite satisfying; small deviations appear at the stagnation points, where the flow speed goes to zero. This test represents one of the lowest margin where the Runge–Kutta scheme, coupled with a compressible Euler solver, can be used in a reasonable manner over an airfoil.

Figure 3(b) shows the pressure coefficient computed for Mach 0.8 and $\alpha = 0^\circ$. This is quite a standard test case often found in the literature. Small differences appear at proximity of the shock region, probably because of artificial dissipation influence. Besides, it is important to note that the code capture very well the trailing edge pressure coefficient distribution,

 

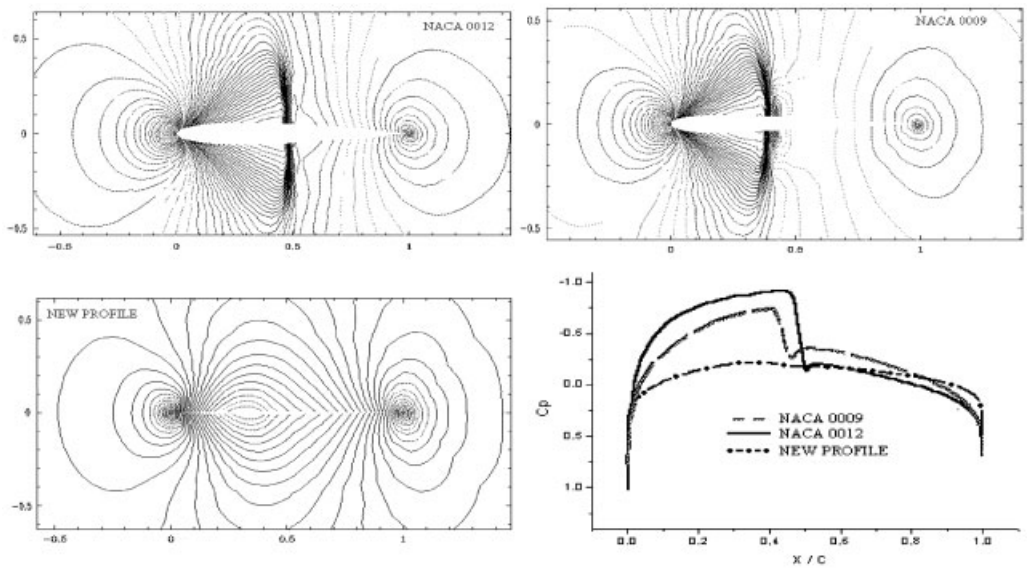


Figure 4. Pressure lines for airfoils NACA 0012, 0009 and new profile, and corresponding pressure coefficients; Mach = 0.8 and $\alpha = 0^\circ$.

were usually appear some spurious oscillations; such was possible because of the use of an appropriate mesh.

Following, the optimization technique is employed to find the NACA 0009 geometry starting with the NACA 0012. Based on the small thickness difference between these geometries no difficulties are expected; for both a shock appears over the airfoil, being symmetric for airfoil placed parallel to free-stream flow direction ($\alpha = 0$). After that, a new configuration for a given $C_p$ and free stream Mach number 0.8 and $\alpha = 0^\circ$ is searched. Pressure lines and $C_p$ values are indicated in Figure 4. Observe that the code was able to obtain a coherent geometry for such pressure distribution; the shock disappeared and the pressure lines followed the expected distribution. Small symmetry deviations appear at proximity of airfoil chord center, which can be controlled choosing a small niveau for convergence (here, $\varepsilon \leqslant 10^{-4}$).

Finally, Figures 5 and 6 show the pressure coefficient over a wing built combining NACA 0012, 0009 and a new airfoil and over a kind of blended wing body configuration. Figure 5(a) shows the pressure lines over the wing formed by a combination of NACA 0012 airfoils. Although the chord/length variation of 15%, the pressure lines distribution over the wing sections showed to be very similar. Figure 5(b), on the other hand, corresponds to the $C_p$ distribution for wing starting with the NACA 0012 and ending with the new profile (from Figure 4), presenting shocks at wing base and no shock at its tip.

The grid used for blended wing body configuration, as shown in Figure 6, contains $120 \times 24 \times 64$ cells and was generated by six sections using seven airfoils: modified NACA 0030 (body centre), NACA 0030, NACA 65024, NACA 65012, NACA 65004 and NACA 0012 (for winglet tip). Overall dimensions were: wingspan, 8.7 m and length, 7.5 m. The first two segments have a length to wide ratio of 0.94 and 0.88, respectively.

 

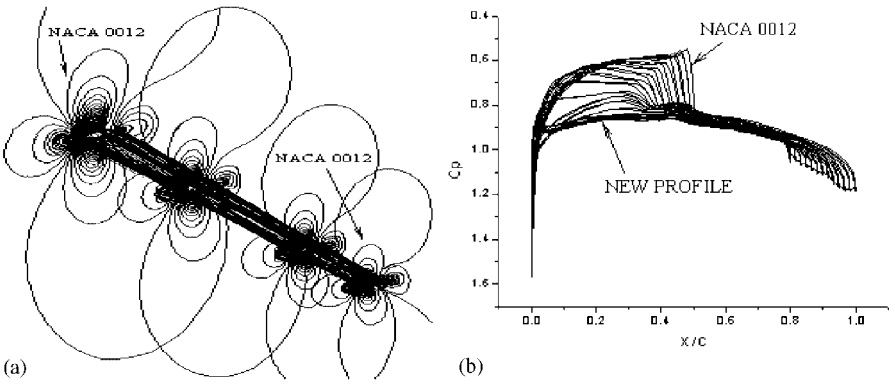


Figure 5. Pressure lines (a) and $C_p$ distribution (b) over wing, Mach $= 0.8$ and $\alpha = 0°$.

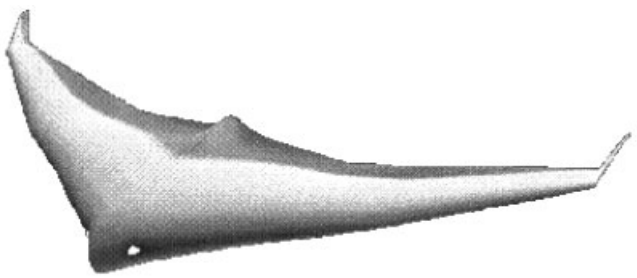

Figure 6. Pressure coefficient for a blended wing body configuration, Mach $= 0.8$ and $\alpha = 0$.

Pressure distribution is similar to that obtained by the wing configuration (Figure 5), unless that the chord variations are very larger in the last case; one can verify the shock-wing interaction over the wing (were white colour changes abruptly). It remembers the geometry of many natural shapes which are motivating the development of many aeronautical new structures.

## 5. CONCLUSIONS

Numerical tests have shown that a method based on the finite volume spatial discretization and the Runge–Kutta time-stepping scheme with preconditioning and multigrid can be helpful to solve (in)compressible fluid flows. Accuracy of the code has been tested when computing compressible and incompressible flows around airfoils [4]. The approach is obviously vectorizable/parallelizable.

The preconditioning used is applicable not only to incompressible flows, but also to compressible flows with incompressible regions. Such a method allows getting the goal of (in)compressible solution of fluid flows. Besides, this preconditioning system has a rate of convergence almost independent from the Mach number.

 

Though the far field effect in the free stream flow, it was necessary to place the outer boundary sufficiently far away (30 chord lengths) from the wing section (airfoil) for almost incompressible flows.

The inverse design, following the elastic membrane technique using Fourier series, showed to be efficient finding new aerodynamical geometries for given pressure coefficient differences. The Fourier series method does not require modification of the flow-field analysis software, converges fast because of its analytical expressions and maintains this behaviour when increasing flow field non-linearities [9].

It is the authors opinion that the comparison among the numerical and theoretical/experimental solutions is encouraging. Therefore, the same code (SCIENT) can be employed to solve compressible as well as almost incompressible three-dimensional flows for situations of technical interest.

## REFERENCES

1. Stuben K, Trottenberg E, Multigrid methods: fundamental algorithms, model problem analysis and applications. *Multigrid Methods*, vol. I, *Lecture Notes in Mathematics*, Springer Verlag: Berlin, 1981.
2. Jameson A, Schimidt W, Turkel E. Numerical solution of the Euler equations by finite volume methods using Runge–Kutta time-stepping schemes. *AIAA Paper* 81–1259, 1981.
3. Choi BD, Merkle CL. Application of time-iterative schemes to incompressible flow. *AIAA Journal* 1985; **23**(10):1518–1524.
4. De Bortoli AL. Multigrid based aerodynamical simulations for the NACA 0012 airfoil. *Applied Numerical Mathematics* 2002; **20**:337–349.
5. Kroll N, Rossow CC. *Foundations of numerical methods for the solution of Euler equations*. Prepared for the Lecture F 6.03 of the CCG, Braunschweig, Germany, 1989.
6. Blazek J. Verfahren zur Beschleunigung der Lösung der Euler- und Navier–Stokes Gleichungen bei Stationären Über- und Hyperschallströmungen. *PhD Thesis*, University of Braunschweig, 1994.
7. Whitfield CL. *Three-dimensional unsteady Euler equation solutions using flux vector splitting*. MS 39762. Mississippi State University, 1983.
8. Dulikravich GS. Shape inverse design and optimization for three dimensional aerodynamics. *AIAA Paper* 95-0695, Reno, Nevada, 1995.
9. Dulikravich GS, Baker DP. Aerodynamic shape inverse design using a Fourier series method. *AIAA Paper* 99-0185, 1999.

 